PHYSICAL REVIEW B **86**, 024438 (2012)

Ordered magnetic dipoles: Controlling anisotropy in nanomodulated continuous ferromagnetic films

Tuhin Maity, Shunpu Li, Lynette Keeney, and Saibal Roy[*]

Tyndall National Institute, University College Cork, Lee Maltings, Dyke Parade, Cork, Ireland

(Received 15 February 2012; published 30 July 2012)

In this paper, the research focus is how to entangle magnetic dipoles to control/engineer magnetic properties of different devices at a submicron/nano scale. Here, we report the generation of synthetic arrays of tunable magnetic dipoles in a nanomodulated continuous ferromagnetic film. In-plane magnetic field rotations in modulated $Ni_{45}Fe_{55}$ revealed various rotational symmetries of magnetic anisotropy due to dipolar interaction with a crossover from lower to higher fold as a function of modulation geometry. Additionally, the effect of aspect ratio on symmetry shows a novel phase shift of anisotropy, which could be critical to manipulate the overall magnetic properties of the patterned film. The tendency to form vortex is in fact found to be very small, which highlights that the strong coupling between metastable dipoles is more favorable than vortex formation to minimize energy in this nanomodulated structure. This has further been corroborated by the observation of step hysteresis, magnetic force microscopy images of tunable magnetic dipoles, and quantitative micromagnetic simulations. An analytical expression has been derived to estimate the overall anisotropy accurately for nanomodulated film having low magnetocrystaline anisotropy. Derived mathematical expressions based on magnetic dipolar interaction are found to be in good agreement with our results.

DOI: 10.1103/PhysRevB.86.024438 PACS number(s): 75.30.Gw

I. INTRODUCTION

One of the most significant challenges in micromagnetic devices is to configure magnetization directions of patterned ferromagnetic films. In polycrystalline materials, this is mainly determined by external environmental effects or geometry[1] due to insufficient long-range microscopic crystalline order. Hence, applications of these materials are widely based on the ability to control the magnetic anisotropy resulting out of spin configuration based on pattern geometry. In recent years, this has been demonstrated for patterned isolated magnetic structures[2–4] and structured continuous magnetic films.[5,6] Such kinds of control open up opportunities for potential applications, such as spintronic devices, magnetic random access memory (MRAM),[7] high-density patterned information storage media,[7,8] and high-precision ultra-small magnetic field sensors.[9] Due to fundamental reasons and potential applications, it is necessary to understand further the magnetic properties of patterned structures in reduced dimensions, while both geometry and crystal microstructure need to be optimized prior to configuring the magnetization.[10] Subsequent investigations further reveal properties, like geometrical frustration, domain wall pining, etc., due to dipolar interaction based on spin configurations.[11,12] Several methods, such as ion irradiation through a mask,[6] selective epitaxy, surface modulation,[13] etc., have been studied to control the magnetization configuration in patterned structures. Among them, surface nanomodulation is preferred for its cost effectiveness and simplicity to engineer spin configuration locally.[14] Furthermore, the optimization of magnetic parameters, such as pattern geometry, film thickness, intrinsic anisotropy, and coercivity, is essential to obtain a controlled anisotropy in a film by nanomodulation. Magnetostatic energy induced by strong nanomodulation forces the spins into local vortices, which is unfavorable for many applications. Thus, the development of a physical model for an optimized modulation is essential to manipulate film anisotropy.

In this paper we discuss the results of anisotropy variation due to magnetic dipole formation in nanomodulated film and detailed micromagnetic simulation study with key symmetry features of nanomodulation-based anisotropy in continuous ferromagnetic thin films. Additional ways to produce different anisotropies are introduced, which have been validated by experimental evidence and analytical derivation. To determine anisotropy variation due to dipole interactions, we performed various magnetometry measurements combined with magnetic force microscopy (MFM) imaging on nanomodulated continuous $Ni_{45}Fe_{55}$ film. Artificially created ordered corrugation produces controllable magnetic dipoles. However, while the external field favors such magnetic dipole alignment, interdipole magnetostatic interaction results in a variation of the effective magnetostatic energy in different directions. This effect translates into in-plane and out-of-plane anisotropy variation depending upon modulation geometry.

II. EXPERIMENTAL DETAILS

A nanomodulated conformal and uniform alloy composition of ferromagnetic $Ni_{45}Fe_{55}$ thin film [Fig. 1(d)] was prepared by an electrodeposition process[15] on patterned substrates fabricated by nanoimprint lithography.[5] A polymethylmethacrylate (PMMA, molecular weight ~230 k) layer of 1 μm thick was spin-coated on a cleaned, 0.5-mm-thick silicon substrate and baked at 100 °C for 10 min in air. Two different silicon stamps with 400/400- and 200/200-nm diameter/separation (D/S) were used to create square arrays of nanoholes. The stamps were placed on the PMMA layer and heated at 160 °C for 30 min with a pressure of 50 bars to generate an array of nanoholes with a depth of 240 nm [Fig. 1(a)]. After cooling down, the stamps were carefully removed, and an array was imprinted on each substrate. An adhesion layer (10-nm Ti) and a 150-nm layer of Au were sputtered on patterned PMMA as a seed layer [Fig. 1(b)].

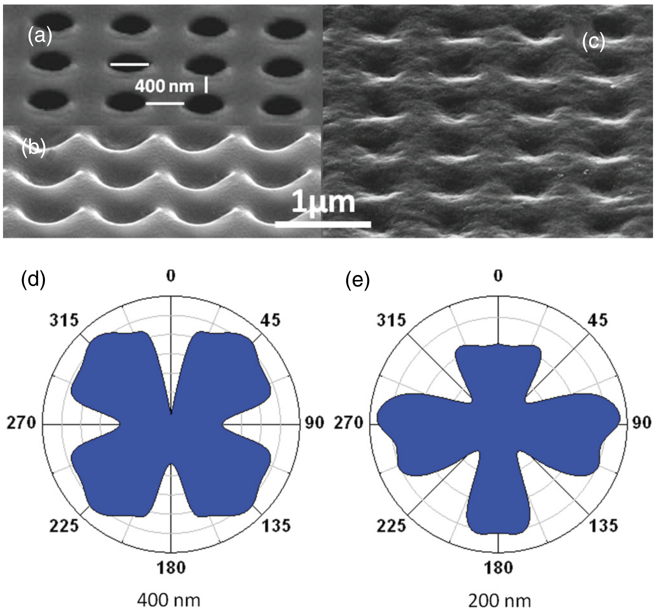

FIG. 1. (Color online) (a) SEM image of nanohole array on PMMA on Si. (b) Gold seed layer on patterned substrate. (c) Electroplated continuous $Ni_{45}Fe_{55}$ on nanomodulated substrate. (d) and (e) Angle-dependent remanant magnetization (M_r vs θ) measured from 3D nanomodulated film with 400-nm and 200-nm element diameter, respectively.

A conformal and uniform alloy composition of $Ni_{45}Fe_{55}$ ferromagnetic film was deposited by electroplating on both types of pattern [Fig. 1(c)]. During the electrodeposition, an external magnetic field was applied at much higher level (∼200 Oe) than the demagnetization field of the film to make sure it produces a uniaxial anisotropy in the deposited film along the field direction ⟨100⟩.

Magnetic properties of nanopatterned films were investigated by using a hysteresis loop tracer (SHB instruments Inc., USA) and SQUID magnetometry (Quantum Design MPMS). A field range of +1000 to −1000 Oe was used to ensure saturation and to measure hysteresis loops in varying in-plane rotational angles.

The existence of magnetic dipoles and their orientation are demonstrated by magnetic force microscopy (MFM) imaging [Fig. 5(e)], where the MFM images were taken at 50-nm distance from sample surface using a commercial atomic force microscope in MFM mode (MFP-3D, Asylum Research) and medium moment MESP-RC probes (Bruker AFM Probes International).

III. RESULTS AND DISCUSSION

We observed that the remanent magnetization (M_r) and coercivity (H_c) both vary as a function of angle due to magnetic anisotropy created by nanomodulation. Since the variation in remanence (M_r) is much stronger than that in coercivity (H_c) for an ultra-soft magnetic material, we consider remanence for further discussion. In Figs. 1(d) and 1(e), normalized remanent magnetization (M_r) is plotted as a function of sample rotation angles with respect to applied in-plane field direction for two different patterns. Both patterns show fourfold symmetry, whereas satellite maxima of the higher order are prominent in 400-nm pattern [Fig. 1(d)], which agrees well with the results of the Object Oriented MicroMagnetic Framework (OOMMF, National Institute of Standards and Technology, USA) simulation.[16] The anisotropy based on nanomodulation is so strong that it could dominate film's uniaxial anisotropy. There is a very minute difference between the remanence magnetization at 0° and 90°, which is due to the influence of uniaxial anisotropy of the film. A novel phase shift is observed in a 200-nm pattern [Fig. 1(e)] for higher aspect ratio, when after gold deposition, the aspect ratio diameter/separation D/S becomes 3:1. The reason for this phase shift will be explained later. In the case of the thickness (t) of the sample being significantly more than the modulation amplitude (A), the anisotropy induced by patterning is dominated by the uniaxial intrinsic anisotropy of the film. When sample thickness $t \sim$ 150 nm is lower than modulation amplitude A (∼240 nm), it tries to form a vortex, and a steplike behavior in a BH curve is visible [Fig. 2(a)]. A further decrease in sample thickness t to ∼50 nm [Fig. 2(b)] gives near zero remanence. The sample with thickness $t \sim$ 150 nm was measured at different temperatures [Fig. 2(c)], which shows the existence of metastable states throughout the temperature range. It is found that the nanomodulated film requires a very high field to reach saturation magnetization due to the formation of magnetic dipoles and their strong coupling. With the change of external magnetic field, the magnetic dipole goes through a transition from stable to metastable state [Fig. 2(c)]. At near zero fields, the remanence M_r suddenly jumps from positive magnetization to negative, which indicates the existence of magnetic dipoles with nonzero M_r. Thus, a complete vortex cannot be achieved in this unique structure. To understand the phenomena, we focus on a single element. For a square array pattern of 400-nm diameter and 100-nm modulation

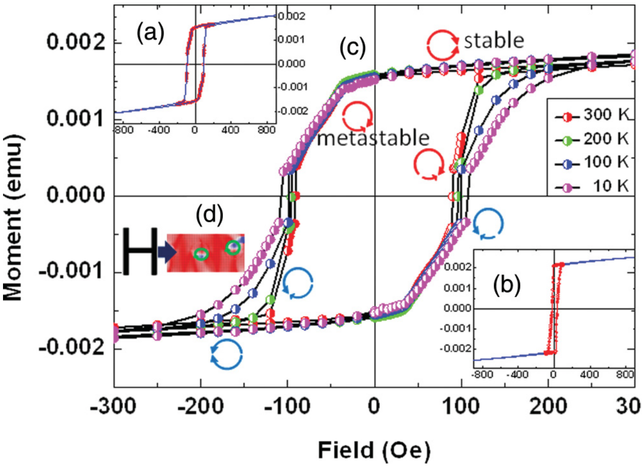

FIG. 2. (Color online) Hysteresis loop measure from thin nanomodulated sample (a) 150 nm and (b) 50 nm, shows metastable state. (c) Steplike MH curve [zoomed of 150-nm thickness] in various temperatures shows existence of metastable dipoles throughout the temperature range. Near zero remanance, the dipoles suddenly jump from positive to negative value. (d) OOMMF simulated picture of magnetization configuration near remanent shows incomplete vortex formation.

amplitude (D/S is 1), the calculated energy densities are 0.49×10^4 and 1.33×10^4 J/m^3 for vortex and near single domain state, respectively. Since the energy of a vortex state is less than that of a near-single-domain remanent state, there should be a strong inclination to adopt vortex states in the nanomodulated continuous ferromagnetic thin films. On the other hand, it is necessary that the demagnetization processes needs to overcome the higher energy barrier to create a local vortex in nanomodulated continuous ferromagnetic thin films where spins are strongly exchanged in parallel due to dipole-dipole interaction. Thus, these dipole interactions in this patterned matrix try to resist formation of vortices, which is analogous to closely packed magnetic dots.[17] As a consequence, a near-single domain state originates at the remanence magnetization state with an intention to become a vortex state. To further elucidate, simulation results [Fig. 2(d)] show that incomplete vortices exist all over the film but in very tiny amounts.

A range of samples with different thicknesses having a fixed modulation amplitude (240 nm) were prepared. Thick film shows uniaxial anisotropy since dipolar anisotropy is weaker compared to uniaxial anisotropy. Very thin film shows only fourfold anisotropy symmetry where dipoles are too weak for higher-order dipolar-interaction. Thus, thickness t near to modulation amplitude A shows maximum anisotropy variation in easy and hard directions. These were further investigated by micromagnetic simulation and discussed later in Sec. IV.

To explain these results, we refer to the recently developed power law for a magnetic film with a roughness-induced demagnetizing effect $H_K \sim \tilde{N} M_S \sim A^2/t$ ($\tilde{N}$ is demagnetizing tensor).[18] Since the power law was derived by using a demagnetizing tensor $\tilde{N}$ for demagnetizing field H_d in a magnetostatic phenomena, it supports the argument that the symmetry of magnetic anisotropy comes from three-dimensional (3D) nanomodulation, which has been shown by means of variation of remanence magnetization. The symmetry is based on the alignment of the pattern-induced magnetic dipoles and their interactions. The direction of effective dipole interaction depends on the direction of applied field. In the MFM image, the dipoles are aligned in $\langle 110 \rangle$ direction as an external field (1000 Oe) was applied in that direction before imaging. In the case of an alignment in a certain direction by an external field [Fig. 5(d)], depending upon the pattern symmetry, dipoles across each patterned element are coupled with their neighbors, and the demagnetization energy decreases with an increase in remanent magnetization due to strong dipole-dipole interactions. Also, the linear density of the dipoles changes as a function of directional angle, and hence the net dipole interaction varies.

The pattern gives both in-plane and out-of-plane modulations [Figs. 5(a)–5(c)], which allow dipoles to rotate. The effective dipole-dipole interaction strength is based on three different parameters: out-of-plane modulation amplitude, in-plane modulation amplitude, and direction, based on modulation geometry and their arrangements.

A possible starting point for the description of the angularly dependent magnetic behavior for this patterned media in terms of anisotropy would be to consider all kinds of anisotropies in a system. We can write an equation for magnetic anisotropy in the following way:

$$H_K(r,\phi,\theta) = \frac{2}{\mu_0 M_S}\left[\frac{K_S V}{2}\sum_{i\neq j}\cos(i)\cos(j) + K_I \sin^2\theta + \sum_n K_n \cos^2(n2\theta) + K_0\right], \quad (1)$$

where the elements in the square bracket are in the following order: (i) global shape anisotropy of the sample, (ii) induced uniaxial anisotropy, (iii) anisotropy due to patterning, and (iv) any other anisotropy. For simulation, we rotated only the pattern to exclude any kind of shape anisotropy. So except for the second and third part, the others remain the same for comparison as a function of angle. We simplify Eq. (1) as follows:

$$H_K(\theta) = \frac{2}{\mu_0 M_S}\left[K_I \sin^2\theta + \sum_n K_n \cos^2(n2\theta)\right]. \quad (2)$$

We generalize a possible directional symmetry where $n = \beta/\alpha$; α is a number representing a minimum geometrical symmetry (i.e., four for square, three for equilateral triangular/hexagonal), and β is a positive integer. Here, K_n denotes the anisotropy constant for the corresponding symmetries. In nanomodulated films, the magnetization follows a wavelike path due to modulation geometry[19] and creates two types of magnetic charge dipoles. Since magnetic induction $\mathbf{B} = \mu_0\,(\mathbf{H} + \mathbf{M})$ do not have divergence, the points where lines of magnetization originate or terminate can be considered as magnetic charge poles with opposite polarity. Looking through the cross section, the magnetization directions are opposite to each other at two sides of an element, which creates out-of-plane dipoles [Figs. 5(a) and 5(b)]. In the case of the in-plane view, magnetization directions at reverse sides of an element are of opposite polarity in an external magnetic field direction, which gives in-plane dipoles [Fig. 5(c)]. These dipoles can interact with each other strongly only when there is a chain of elements in the applied field directions, creating an anisotropic magnetization throughout the whole film. We consider all types of magnetic interaction in different regions and by using sum rules given by Yafet *et al.*[20] The total magnetostatic energy is given by $E_{\text{mag}} = E^x_{\text{mag}} + E^y_{\text{mag}} + E^z_{\text{mag}} = (\frac{1}{2})4\pi M_S^2 V A$, where M_S is the saturation magnetization, V is the volume, and A is modulation amplitude. Since by symmetry $E^x_{\text{mag}} = E^y_{\text{mag}} = E^{\parallel}_{\text{mag}}$, magnetostatic energy becomes $E_{\text{mag}} = E^{\perp}_{\text{mag}} + 2E^{\parallel}_{\text{mag}} = (\frac{1}{2})4\pi M_S^2 V A$. For an externally applied field H, the magnetostatic energy can be written as $E_{\text{mag}} = \int -\frac{1}{2}\vec{M}\cdot\vec{H}dv$. We can consider two different layers of the pattern with magnetic and nonmagnetic regions in each layer. The magnetization can be written as $M = M_1^U + M_2^U + M_1^L + M_2^L$ for an applied field $H = H_1^U + H_2^U + H_1^L + H_2^L$ ($U \sim$ upper layer, $L \sim$ lower layer, 1 is magnetic region, and 2 is nonmagnetic region) for four different cases. Then we can write magnetostatic energy in the following way for patterned structure:

$$E_{\text{mag}} = \sum_{n,m}\int -\frac{1}{2}\vec{M}^{j}_{i\;n,m}\cdot\vec{H}_{n,m}dv, \quad (3)$$

where the distribution of magnetization can be expanded in Fourier series as follows:

$$M(x,y) = \sum_{n=0}^{+\infty}\sum_{m=0}^{+\infty} M_{i\ \ n,m}^{j} \sin(k_n x)\sin(k_m y), \tag{4}$$

and the field corresponding to each magnetization will be $divH_i^j = -4\pi divM_i^j$.

The interlayer interaction gives perpendicular anisotropy, and the remaining effects give in-plane anisotropy. Rewienski[21] found magnetic anisotropy of ferromagnetic thin films due to surface roughness. Using the same principle, we have calculated the anisotropy energy due to each single element as $E_{\text{mag}}^{\|} = C_i(\frac{1}{2})M_S^2(\frac{1}{4})[A\{1 - f(2\pi\frac{A}{D})\}]$ and $E_{\text{mag}}^{\perp} = C_i(\frac{1}{2})M_S^2(\frac{1}{2})[-A\{1 - f(2\pi\frac{A}{D})\}]$, where C_i is a constant which depends on pattern geometry and aspect ratio. The function[20] f is 0 at $A/D = 1$ and 1 at $A/D = 0$ [Fig. 5(f) inset]. The dipolar anisotropy is given by $E_{da} = E_{\text{mag}}^{||} - E_{\text{mag}}^{\perp} \neq 0$, which gives a finite dipolar anisotropy energy depending upon the modulation geometry. Considering up to second-order harmonics, we can rewrite the dipolar anisotropy for anisotropy energy as $K^S = C_i(\frac{1}{2})4\pi M_S^2(\frac{3}{4})A[1 - f(2\pi\frac{A}{D})]$, where A is the amplitude of modulation and D is the diameter of the element. The dipole-dipole interaction strength depends on the density of elements in a particular direction. So we add another term sin $(90^\circ/\beta)$ for pattern induced magnetic anisotropy.

Using the expression for K^S, we can then rewrite Eq. (1)

$$H_K(\theta) = \frac{2}{\mu_0 M_S}\sum_n CA\left[1 - f\left(2\pi\frac{A}{D}\right)\right]\left\{\sin\left(\frac{90^\circ}{\beta}\right)\right\} \times \cos^2\left(\beta\frac{2\theta}{\alpha}\right), \tag{5}$$

where $n = \beta/\alpha$, and the constant C depends upon single-element geometry and diameter/separation D/S. This equation describes the possibility of anisotropy variation by nanomodulation geometry for different ferromagnetic materials.

IV. MICROMAGNETIC SIMULATION

The experimental results for nanomodulated continuous ferromagnetic thin film has further been investigated by static micromagnetic simulations, which were carried out by solving the Landau–Lifshitz–Gilbert (LLG) equations $\frac{\partial\vec{M}(\vec{r},t)}{\partial t} = |\gamma|\vec{M}(\vec{r},t) \times H_{\text{eff}}(\vec{r},t) + \alpha/M_S[\vec{M}(\vec{r},t) \times \frac{\partial\vec{M}(\vec{r},t)}{\partial t}]$ and $H_{\text{eff}}(\vec{r},t) = -(\frac{1}{\mu_0})[\frac{\partial E}{\partial\vec{M}(\vec{r},t)}]$ using OOMMF[16] software. Square and equilateral triangle arrays were made of 7 × 7 circular elements [Fig. 3(a)] as this is the minimum number of elements required to include long-range magnetostatic interaction effects on a large scale.[22] For simulation, the cubic cell is used, and minimum length of the cubic cell was taken as 6.25 nm, which is nearly equal to exchange length $(A/2\pi)^{1/2}M$, where A is exchange constant, and M is magnetization. The total number of cells (102 400 $\sim 10^5$) was constant for all simulations to maintain the same geometrical accuracy, while the cell dimensions were varied depending upon simulation parameters. The 65% area of the middle of the substrate was patterned to avoid edge effects.

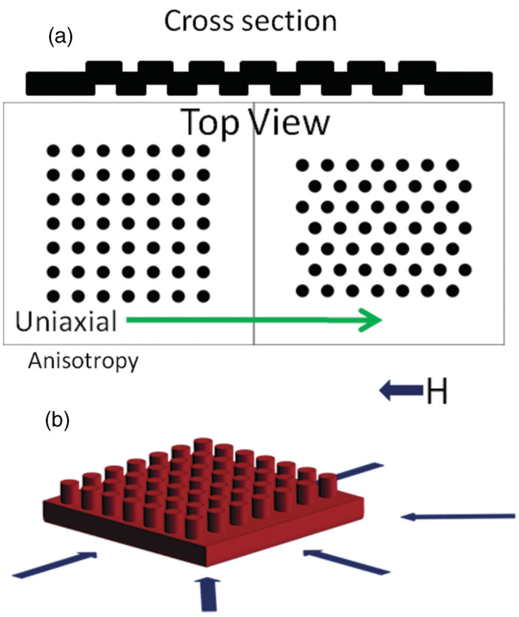

FIG. 3. (Color online) (a) Cross section and top view of patterned film used for simulation. (b) Schematic diagram of rotation of H_{ext} in x-y plane. Uniaxial anisotropy in ⟨100⟩ direction of the pattern is considered for all simulation.

We assumed typical material parameters for $Ni_{45}Fe_{55}$: $4\pi M_S = 1.2 \times 10^6$ A/m, $A = 6.47 \times 10^{-12}$ J/m, and anisotropy constant $K = 600$ J/m^3 in the ⟨100⟩ direction of the pattern [Fig. 3(a)]. The global external magnetic field H_{ext} was applied in the ⟨100⟩ direction of the whole atlas. To study rotational symmetry, we only rotated the pattern [Fig. 3(b)] with respect to the whole atlas background and applied a magnetic field to confirm that only the effect of the patterned area was taken into account. In these calculations, we did not include the simulated results of angles near 0°, 90°, and its equivalent angles for the square pattern to avoid artificial degeneracy arising in simulations, when H_{ext} is exactly parallel to the ⟨100⟩ and ⟨010⟩ directions. The external applied magnetic field H_{ext} was increased from 0 to 400 Oe on the film to ensure saturated static magnetization (H_K).

For a single element, we simulate the structure with cell dimension 20 × 20 × 20 nm of 400-nm pattern elements having 3 × 3 arrays, as this is the minimum number of elements required to include short-range magnetostatic interaction effect.

The pattern diameters are varied from 50 to 800 nm, while the modulation amplitude was held constant at 100 nm. Since at first approximation the magnetostatic energy (E_M) is inversely proportional to the remanent magnetization M_r (i.e., $E_M \sim H_K \sim 1/M_r$), the polar plot of simulated results is plotted with the opposite polarity, which is defined by $1 - E_M$. This indicates the angle dependence of normalized magnetostatic energy E_M at a single domain state, which in turn leads to an angular dependence of remnant magnetization M_r. The simulation results based on pattern diameter variation are shown in Fig. 4, where the remanent magnetization is plotted as a function of the angle of the applied field. To amplify the variation in magnetization, the remanent magnetization is

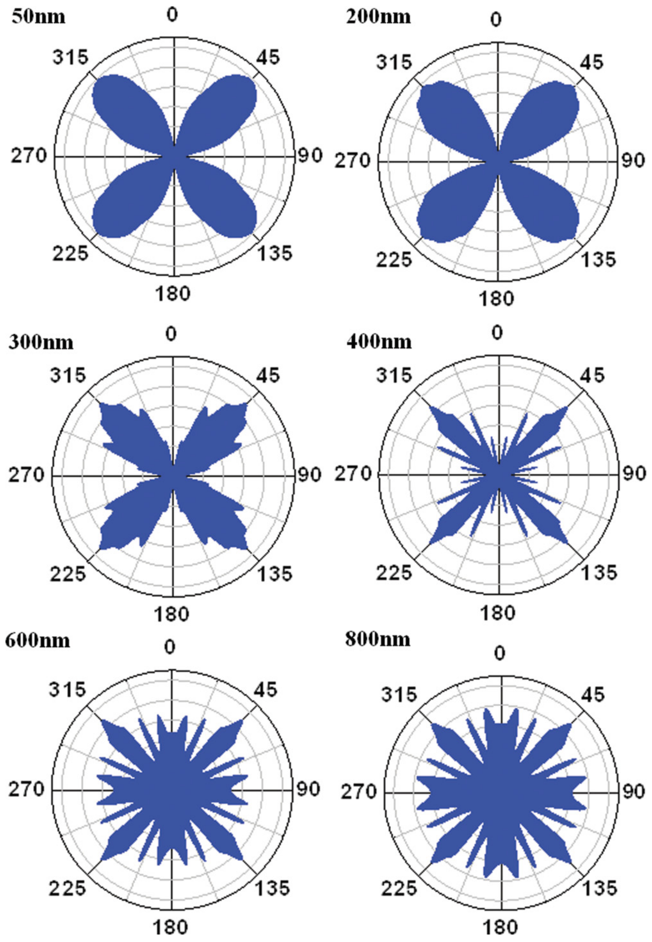

FIG. 4. (Color online) Simulated angle dependence of magnetostatic energy in nanomodulated films for different pattern diameter (D) from 50 to 800 nm plotted in inverse polarity. All of the plots certainly show fourfold symmetry. Hints of new eightfold peaks at 300 nm, 12-fold peaks at 400 nm superimposed on the fourfold ones are seen. Higher-order peaks are observed in bigger diameter. The modulation amplitude (A) 200 nm remained the same for all diameters. Further decrease of modulation amplitude shows the same type of result (symmetry increase).

normalized. Variation of diameter and modulation amplitude shows a clear trend of symmetry variation. All of the plots in Fig. 4 certainly show fourfold symmetry. There is the indication of new eightfold peaks at 300 nm, superimposed on the fourfold ones, and these become clearer at 400 and 600 nm. The influence of symmetries has been plotted in Fig. 6(e), which shows that only $4n$ symmetries [$360^\circ/\theta =$ symmetry, Fig. 5(d)] are available in a square pattern. Hence, controllable ($4n$-fold) symmetry can be obtained in a square array pattern. This signifies that the nanomodulation minimizes the magnetostatic energy at least in the two equivalent $\langle 110\rangle$ directions, where the uniaxial anisotropy (induced in the $\langle 010\rangle$ direction during simulation) has been dominated by the anisotropy due to nanomodulation. For the smaller diameters ($\sim$50 nm), this fourfold symmetry is dominant, whereas satellite maxima beside each main maximum ($\langle 110\rangle$ direction) become visible as the pattern diameter increases or modulation amplitude decreases. In a continuous patterned film, the coupling between the periods of the nanostructures is much stronger rather than interdot coupling between isolated two-dimensional (2D) dot arrays, which increases the anisotropy.[23] Thus, an eightfold or even higher-order symmetry may contribute to the anisotropy considerably. In the case of the high aspect ratio substrate, the wavelike modulation of magnetic domains is envisaged to shift to the upper region [Fig. 5(a)]. Here, the modulation amplitude is more in the $\langle 110\rangle$ direction than in the $\langle 100\rangle$ direction, and the hard axis is obtained in the $\langle 110\rangle$ direction, which is supported by simulation result [Fig. 6(a)]. Same kinds of results should occur in the case of low aspect ratio, where wavelike modulation shifts to the lower part of the modulated film [Fig. 5(b)]. Variation of diameter and modulation amplitude shows a clear trend of symmetry ($4n$-fold) variation. Similarly, other types of symmetries can be obtained by changing the pattern or dipole arrangement.

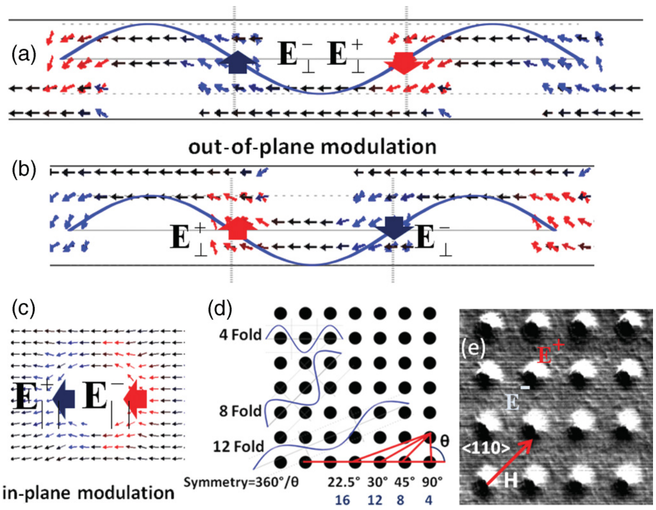

FIG. 5. (Color online) Schematic diagram of (a)–(b) out-of-plane and (c) in-plane modulation shows formation of dipoles and (d) direction array chain of dipole-dipole interactions. Modulation switches to (a) upper layer for high aspect ratio and to (b) lower layer for low aspect ratio. (d) Different symmetry formation due to pattern arrangement has been shown. (e) MFM phase images of dipoles. An external field of 1000 Oe was applied in $\langle 110\rangle$ direction before imaging. The images were taken at a 50-nm distance from sample surface.

The derived anisotropy equation [Eq. (5)] fits well with our simulated results and describes possible anisotropies for different ferromagnetic materials. We considered up to 16-fold symmetry in curve fitting, which fits well to the data at lower diameter ($\sim$50 nm) and near that [Fig. 6(c)], but does not fit well at higher diameters (D) [Fig. 6(d)], which indicates the dominance of lower-order symmetry in lower diameters. The demagnetization energy density (calculated from simulated results) as a function of pattern geometry, follows function[21] f, which delineates the fact that the uniaxial induced anisotropy is strongly dominated by the anisotropy created by nanomodulation [Fig. 6(f)]. Simulation of the triangular pattern shows a $3n$-fold symmetry [Fig. 6(b)], which supports the generalized model including all possible different symmetries.

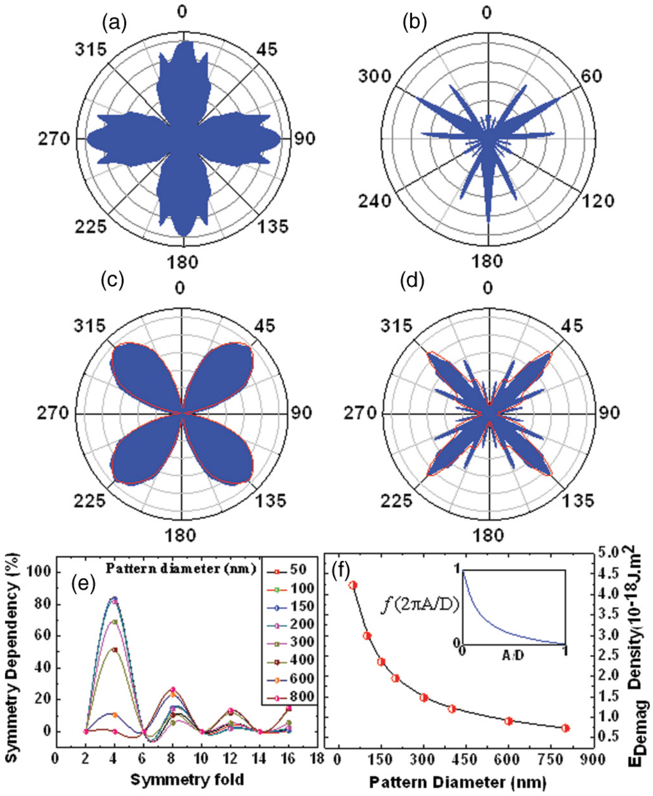

FIG. 6. (Color online) (a) For closed-packed array, phase shift has been observed. (b) Equilateral triangular array shows $3n$-fold symmetry. Fitted curve (red line) for (c) 200-nm and(d) 400-nm pattern with derived generalized anisotropy equation [Eq. (3)]. (e) Symmetry dependency for different pattern diameters, (f) geometry depended demagnetization energy. Inset graph shows the behavior of f as a function of A/D.

V. CONCLUSION

In conclusion, we have explored the variation of magnetic anisotropy through the formation of magnetic dipoles in continuous ferromagnetic thin films due to a unique nanomodulation. Experimental evidence of well-ordered dipoles with metastable state have been detected by means of variation of magnetic anisotropy, step hysteresis, and MFM imaging. The novel 3D modulation generates both in-plane and out-of-plane dipoles, where the competition between in-plane and out-of-plane dipoles creates metastable state, giving opportunity to manipulate anisotropy. The anisotropy model, based on collective dipolar interaction, is used to demonstrate the ability to control anisotropy in continuous ferromagnetic thin films by minimizing magnetostatic energy through nanomodulation. The change of diameter/separation ratio D/S in nanomodulation can switch the anisotropy direction due to the transformation of the modulation wave from one layer to another layer. The generalized model helps us to find out possible anisotropy based on material property and geometrical arrangement of nanopattern. By varying amplitude/diameter A/D ratio and geometrical arrangement α, one can achieve desired anisotropy. Thicknesses close to the modulation amplitude provide more control over the anisotropy. Additionally, the formation of a metastable single domain resists vortex formation in nanopatterned ferromagnetic thin films, which is essential for realizing devices, such as volatile memory, magnetically frustrated patterned media,[11] highly integrated nanoscale magnetic devices,[24,25] etc. Fourier analysis of magnetostatic energy for this nanomodulated film supports the existence of magnetic diploes ($E_{da} \neq 0$). The derived generalized mathematical expression based on magnetic dipolar interaction is found to be in good agreement with our results, which can help to estimate and understand the anisotropy in other pattern media also. The method described in this paper is much simpler and can be demonstrated at a larger scale.

ACKNOWLEDGMENTS

The authors gratefully acknowledge the financial support from EU FP7 Network of Excellence (NoE) project "NANOFUNCTION" Grant No. 257375, Science Foundation Ireland (SFI) Principal Investigator (PI) Project No. 11/PI/1201 and the partial support of SFI under the FORME Strategic Research Cluster Award No. 07/SRC/I1172. T.M. acknowledges Jeffrey Godsell for initial assistance on micromagnetic simulation.

---

[*] Corresponding author: saibal.roy@tyndall.ie

[1] J. Briones, F. Montaigne, D. Lacour, G. Lengaigne, S. Girod, and M. Hehn, Appl. Phys. Express **3**, 073002 (2010).

[2] R. Skomski, H. P. Oepen, and J. Kirschner, Phys. Rev. B **58**, 11138 (1998).

[3] S. P. Li, D. Peyrade, M. Natali, A. Lebib, Y. Chen, U. Ebels, L. D. Buda, and K. Ounadjela, Phys. Rev. Lett. **86**, 1102 (2001).

[4] R. P. Cowburn, D. K. Koltsov, A. O. Adeyeye, M. E. Welland, and D. M. Tricker, Phys. Rev. Lett. **83**, 1042 (1999).

[5] S. P. Li, J. F. Godsell, and S. Roy, J. Appl. Phys. **108**, 093915 (2010).

[6] C. Chappert, H. Bernas, J. Ferre, V. Kottler, J. P. Jamet, Y. Chen, E. Cambril, T. Devolder, F. Rousseaux, V. Mathet, and H. Launois, Science **280**, 1919 (1998).

[7] S. Tehrani, E. Chen, M. Durlam, M. DeHerrera, J. M. Slaughter, J. Shi, and G. Kerszykowski, J. Appl. Phys. **85**, 5822 (1999).

[8] F. Nguyen-Van-Dau, M. Sussiau, A. Schuhl, and P. Galtier, J. Appl. Phys. **81**, 4482 (1997).

[9] R. P. Cowburn, D. K. Koltsov, A. O. Adeyeye, and M. E. Welland, J. Appl. Phys. **87**, 7082 (2000).

[10] M. Hehn, K. Ounadjela, R. Ferré, W. Gramge, and F. Rousseaux, Appl. Phys. Lett. **71**, 2833 (1997)

[11] Y. S. Jung, W. Jung, and C. A. Ross, Nano Lett. **8**, 2975 (2008).

[12] E. Mengotti, L. J. Heyderman, A. F. Rodríguez, F. Nolting, R. V. Hügli, and H. B. Braun, Nat. Phys. **7**, 68 (2011).

[13] D. J. Twisselmann, P. G. Chambers, C. A. Ross, G. Khanna, and B. M. Clemens, J. Appl. Phys. **92**, 3223 (2002).

[14] W. Oepts, M. A. M. Gijs, A. Reinders, R. M. Jungblut, R. M. J. van Gansewinkel, and W. J. M. de Jonge, Phys. Rev. B **53**, 14024 (1996).

[15] S. Roy, A. Connell, M. Ludwig, N. Wang, T. O'Donnell, M. Brunet, P. McCloskey, C. ÓMathúna, A. Barman, and R. J. Hicken, J. Magn. Magn. Mater. **290-291**, 1524 (2005).

[16] M. Donahue and D. G. Porter, *OOMMF User's Guide*, Version 1.0, Interagency Report NISTIR 6376 (National Institute of Standard and Technology, Gaithersburg, 1999), http://math.nist.gov/oommf.

[17] Y. P. Zhao, R. M. Gamache, G. C. Wang, T. M. Lu, G. Palasantzas, and J. T. M. D. Hosson, J. Appl. Phys. **89**, 1325 (2001).

[18] Y. P. Zhao, G. Palasantzas, G. C. Wang, and J. T. M. De Hosson, Phys. Rev. B **60**, 1216 (1999).

[19] R. P. G. McNeil, Nano Lett. **10**, 1549 (2010).

[20] Y. Yafet, E. M. Gyorgy, and L. R. Walker, J. Appl. Phy. **60**, 4236 (1986).

[21] M. Rewienski, Acta Phys. Pol. A **88**, Supplement, S-69 (1995).

[22] K. Y. Guslienko, V. Novosad, Y. Otani, H. Shima, and K. Fukamichi, Phys. Rev. B **65**, 024414 (2001).

[23] K. Y. Guslienko, Phys. Lett. A **278**, 293 (2001)

[24] H. Watanabe, C. Manabe, T. Shigematsu, and M. Shimizu, Appl. Phys. Lett. **78**, 2928 (2001).

[25] F. J. Castano, D. Morecroft, W. Jung, and C. A. Ross, Phys. Rev. Lett. **95**, 137201 (2005).